High-resolution ^{133}Cs 6*S*–6*D*, 6*S*–8*S* two-photon spectroscopy using an intracavity scheme

You-Huan Chen,[1] Tze-Wei Liu,[1] Chien-Ming Wu,[1] Chien-Chung Lee,[1] Chao-Kuei Lee,[2] and Wang-Yau Cheng[1,*]

[1]*IAMS, Institute of Atomic and Molecular Science, Academia Sinica, Taiwan*

[2]*Institute of Electro-Optical Engineering and Semiconductor Technology Research and Development Center, National Sun Yat-Sen University, Taiwan*

**Corresponding author: wycheng@gate.sinica.edu.tw*

Received September 10, 2010; revised November 13, 2010; accepted November 18, 2010; posted December 2, 2010 (Doc. ID 134939); published January 5, 2011

This Letter presents an intracavity scheme for diode laser based two-photon spectroscopy. To demonstrate generality, three ^{133}Cs hyperfine transition groups of different wavelengths are shown. For the 6*S*–6*D* transitions, we achieved a 10^2 times better signal-to-noise ratio than in previous work [J. Phys. Soc. Jpn. **74**, 2487 (2005)] with 10^{-3} times less laser power, revealing some previously vague and unobserved spectra. Possible mutual influences between the two-photon absorber and laser cavity were investigated for the first time to our knowledge, which leads to the application of a reliable hand-sized optical frequency reference. Our approach is applicable for most of the two-photon spectroscopy of alkali atoms.

OCIS codes: 120.3930, 300.6210, 300.6190, 300.6320.

High signal-to-noise spectra of direct two-photon transitions where one-photon detuning is far from the intermediate state is resolved with difficulty using a low-power 100 kHz linewidth laser. Taking cesium/rubidium atom two-photon transitions as examples, people have employed a high-power Ti:sapphire laser [1,3–7], cavity-enhanced scheme [5–7], or a tapered amplifier [8] to boost the laser power in order to improve the spectral signal-to-noise ratio (SNR). However, these methods necessitate increased complexity or cost. Our report demonstrates success of high-resolution two-photon spectroscopy using simply a low-power external-cavity diode laser [9] with an intracavity Cs cell (intracavity scheme). To show generality, we demonstrated our results for three transition groups, namely, ^{133}Cs $6S_{1/2} \rightarrow 6D_{3/2}$ (885.4 nm), $6S_{1/2} \rightarrow 6D_{5/2}$ (883.7 nm), and $6S_{1/2} \rightarrow 8S_{1/2}$ (822.5 nm) hyperfine transitions. For the 6*S*–6*D* transitions, we achieved 2 orders of magnitude better SNR than previous work [1,2], with 3 orders of magnitude less laser power, revealing some previously vague and unobserved spectra. Our resolved two-photon spectroscopy offers several advantages in laser stabilization; namely, the high-resolution spectrum provides good optical frequency discrimination, the weakly induced quadrupole moment yields no perturbation, within our measurement precision, to the laser cavity, and the complete beam overlapping further eliminates the Doppler background.

Although installing an absorber inside the laser cavity for saturation spectroscopy has been performed for decades, the inevitable mutual interactions between the laser cavity and the absorber distorted the spectral shape and thus limited the applications [10–14]. Yet to our knowledge, intracavity cesium two-photon spectroscopy has not been investigated. Our study focuses on intracavity two-photon spectra and their lineshape symmetry, and pressure shift, clarifying the possible influences between the absorber and laser cavity and demonstrating the application for laser stabilization. Our simple high-resolution approach should be applicable to the two-photon spectroscopy of alkali atoms.

The structure of our intracavity two-photon stabilized laser is illustrated in Fig. 1. It was vital, though challenging, to build a quiet, mode-hop-free optical resonator at 23 °C, while hosting an intracavity cesium cell heated to 100 °C, all within a range of 1 mK temperature instability. However, once all the parameters, such as cavity length, thermal materials, and temperature settings, are determined, it was not difficult to duplicate more systems. Such a tight temperature control efficiently minimized the cavity-length drift and provided laser stabilization for several weeks. Two diode lasers of different wavelengths were used in two slightly different laser systems. As labeled by "A," the 884 nm system used a 40 mW output power diode (AR coated), and the 822 nm system used a 100 mW output power diode (Fabry–Perot type). Fine wavelength tuning was achieved by a conventional Littrow scheme [9] with a 1800 grooves/mm grating. The grating, indicated by "B," was properly oriented so that 45% (95%) of laser power could be diffracted back

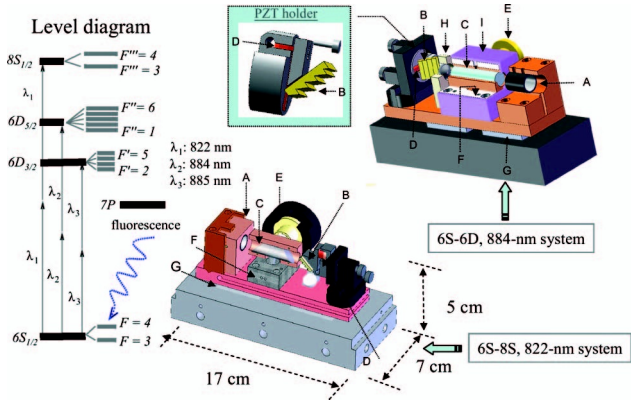

Fig. 1. Structure of our intracavity two-photon stabilized lasers and the relevant energy level diagram: A, copper-housed laser diode with a collimating tube; B, 1800 groove/mm grating; C, AR-coated cesium cell (884 nm system) and Brewster-window sealed cesium cell (822 nm system); D, piezoelectric transducer; E, fluorescence collector; F, Teflon bulk for thermal isolation; G, TE cooler; H, focus lens and holder; and I, μ-metal. Inset, enlargement of PZT holder for the 884 nm system.

to the laser cavity for an 884 nm (or 822 nm) diode laser system, eventually yielding 10 mW (or 2 mW) zero-order output power, respectively. The laser power inside the laser cavity was thus estimated as 18 mW (or 40 mW). A quartz cell with AR-coated windows was used for the 884 nm laser system, and a Brewster-window sealed cell was used for the 822 nm laser system, labeled "C." An additional lens in the 884 nm laser system, labeled "H," together with the other lens located in the collimating tube (A), was used to focus the laser beam into the center of the cesium cell to provide sufficient power density (~35 mW/mm^2) inside the cesium cell, while only one collimating lens was needed for the 822 nm system (~40 mW/mm^2). A layer of μ-metal, labeled "I" and shown in purple, was added around the whole cell of the 884 nm system to provide shielding from the magnetic field of the Earth. We found the linewidth was 1.2 MHz broadened ($F = 4 \rightarrow F'' = 6$, $D_{5/2}$) without shielding the magnetic field of the Earth, and more layers did not further reduce the linewidth, under our measurement precision. When laser stabilization was activated, the diode laser was frequency modulated by a dither on the diode current, and the error signal from the photomultiplier tube was retrieved following a standard demodulation procedure with a homemade lock-in amplifier.

Figure 2 shows, from left to right, absorption spectra of $6S_{1/2}$–$6D_{5/2}$ transitions, derivativelike signals of $6S_{1/2}$–$6D_{3/2}$ transitions, and one absorption signal of $6S$–$8S$ transition, respectively. The best SNR of all transitions is similar, and all good for laser stabilization. The intracavity absorption signals (from a lock-in amplifier) in which chopping fluorescence was realized by modulating the driving current of the diode laser with a 30 kHz square wave, resulting in a 50 MHz optical frequency jump between the absorption center and the nonfluorescence region. The hand-sized laser in the right side of Fig. 2 ($6S$–$8S$) was freely running around the spectral center. Because of the high resolution, some spectra were clearly resolved for the first time, namely, $F = 4 \rightarrow F'' = 2$ and $F = 3 \rightarrow F'' = 1$ of $6S_{1/2} \rightarrow 6D_{5/2}$. The frequency axis of Fig. 2 was calibrated to a transition

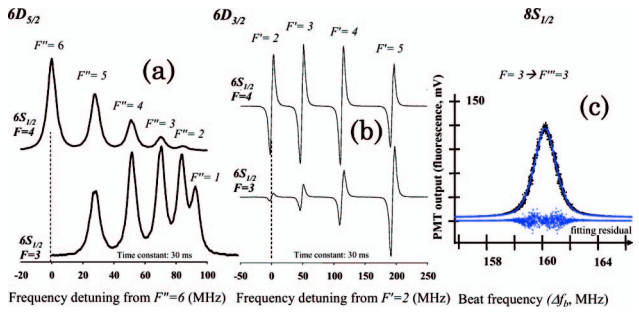

Fig. 2. Intracavity Doppler-free two-photon spectrograms in three different wavelengths and the corresponding level diagram. (a) Typical absorption signals ($6S_{1/2}$–$6D_{5/2}$, 883.7 nm). Note that $F'' = 2$ of $F = 4$ group and $F'' = 1$ of $F = 3$ group are clearly resolved. (b) Typical first derivative signals ($6S_{1/2}$–$6D_{3/2}$, 885.4 nm). (c) Isolated $6S_{1/2}$–$8S_{1/2}$ (822.5 nm) hyperfine transition for inspecting the influence of laser cavity on the spectral lineshape. The hand-sized laser on the right side was freely running; see text. The blue line in the right-side figure is a Voigt-fitting curve. The symmetric residual is a sufficient condition for lineshape symmetry.

resonance of the largest SNR in their group. For example, we chose $F'' = 6$ transition for the frequency axis reference of $6S_{1/2}$, $F = 4 \rightarrow 6D_{5/2}$ group, and we chose the same transition as the frequency axis reference of $6S$–$8S$ group. This was achieved by recording the beat note (Δf_b) between our hand-sized diode laser and the other frequency-stabilized 884 nm (822 nm) laser, for which the laser frequency was not modulated [8]. Note that a 160 MHz frequency difference of Fig. 2(c) was from a frequency bridge by a double-pass acoustic-optical modulator system [8]. For studying the possible influence of laser cavity on the lineshape symmetry, we employed a symmetric function (Voigt) to fit the isolated $6S$–$8S$ transition [Fig. 2(c)], since it is about 4 GHz away from the nearby transition. The fitting residuals show a highly symmetric structure, which is a sufficient condition to show the symmetry of the experimental lineshape. We conclude that the influence of laser cavity on the two-photon transition is slight compared with the observations in dye laser intracavity spectroscopy conducted by Hill III, *et al.* [10]. The hyperfine interval fitting is 1 order of magnitude better than previous work [1,3,4]. The major factors for the weak influences on lineshape symmetry are attributed to the flat laser gain profile, gas-lensing free and mode pulling free (within our measurement precision). Mode pulling is a troublesome issue for intracavity one-photon spectroscopy [11,12] and was inspected here by observing the possible lead-lag of the laser frequency. Laser frequency lead-lag, caused by the dispersion of the gain/absorption medium [12], is nonlinearly dependent on the physical length of the laser resonator. To observe the mode pulling effect caused by two-photon absorption, we recorded Δf_b synchronously with each saw-wave voltage, because Δf_b is related to the cavity optical length and the saw-wave voltage is related to the physical length. This was done by imposing a constant-frequency saw wave (10 mHz) to change the offset point of the PZT feedback loop while the laser frequency locking was kept engaged. The maximum voltage of saw wave was 0.3 V. Figure 3 illustrates the response of laser frequency (Δf_b) versus each

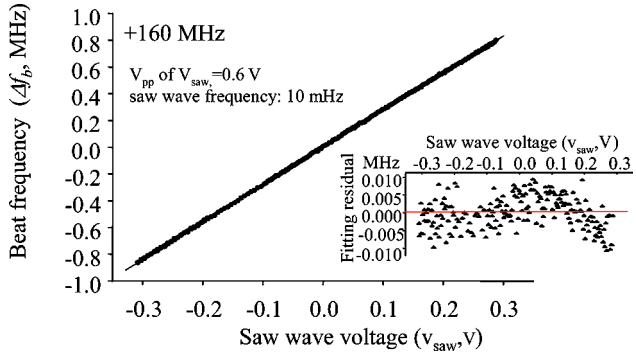

Fig. 3. Mode pulling inspection, $6S$–$8S$, $F = 3 - F'''' = 3$ transition was selected. Δf_b is the beat frequency of the two lasers, and V_{saw} is the offset voltage of the cavity PZT with a constant 10 mHz saw-wave frequency; frequency locking was always engaged during the period of data acquisition. Data points were repeatedly obtained by scanning the laser cavity length with a slow saw wave (10 mHz) and recording each point of the saw-wave voltage versus Δf_b simultaneously. The red line is a linear fitting. The fitting residual mainly comes from laser frequency instability during the scan; see text.

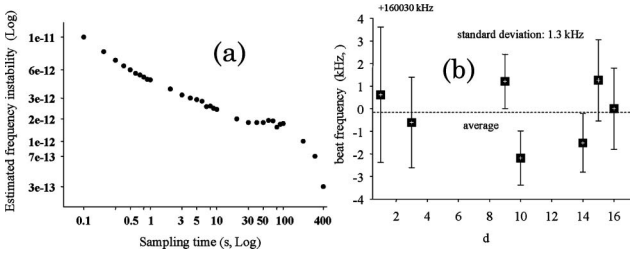

Fig. 4. Demonstration of laser stabilization. Two hand-sized $6S$–$8S$, $F = 3 - F''' = 3$ transition-stabilized lasers were used. (a) Stability: here the "frequency instability" is deduced via a process similar to the Allan deviation; however, it was not exactly an Allan deviation due to our lambda-type counter [15]; see text. Both horizontal and vertical axes are on a log scale. Frequency instability was estimated as 3×10^{-13} ($\Delta f \sim 100$ Hz) at a 400 s sampling time. (b) Reproducibility: beat note measurements over a period of 16 d. A maximum frequency discrepancy of 3.5 kHz was observed.

cavity-length changing (saw-wave voltage). The red line is a linear fitting to the data points. The fitting residual was within the frequency instability (10 kHz) when the laser frequency was detuned. Therefore, we concluded that the nonlinear mode pulling effect was not observed within our 10 kHz measurement uncertainty. To directly observe the possible gas-lensing effect [13,14], which might vary the laser output power and the beam size, we compared the laser output power and beam size when the laser is frequency-stabilized to, or detuned far from, the two-photon transition. Our measurements showed no evidence of any lensing effect—within the power measurement uncertainty of 10 μW and size measurement uncertainty of 0.05 mm. Details of the laser stabilization are given in Fig. 4. The estimated Allan deviation [15] was deduced from a beat note measurement with two hand-sized cesium $6S$–$8S$, $F = 3 - F''' = 3$ transition-stabilized lasers. In Fig. 4(a) we show the achieved laser frequency instability of $\sim 3 \times 10^{-13}$, or $\Delta f \sim 100$ Hz, at a 400 s sampling time. Note that Fig. 4(a) is just an estimated value because our lambda-type counter could not really provide appropriate sequences of frequency counting for directly deducing the Allan variance [15]. Reproducibility was estimated by tracking the frequency deviation of two independent lasers stabilized to the same two-photon transition for 16 d, as displayed in Fig. 4(b). The modulation and pressure shifts of $6S$–$8S$, $F = 3 - F''' = 3$ transition were measured to be 3 kHz/MHz linear shift and –290 kHz/Pa with $\sim 7 \times 10^{11}$ (atom/cm^3) atom density, respectively, which differed from [8,16] owing to different cell wall materials, residual magnetic field, and resolved spectral width.

Higher spectral quality will lead to higher accuracy on spectral positions. Our curve fitting in Fig. 2 showed promise for precisely fitting the hyperfine coupling constants of the cesium $6S$–$6D$ transition to determine the magnetic octupole of the cesium nucleus [17], which will help for clarifying the puzzle between the atomic physics observation and nuclear modeling [17]. Moreover, because the 822 and 884 nm wavelengths are within the gain profile of the Ti:sapphire laser, the two compact lasers in this report will be used for two frequency references of our mode-lock laser system for directly stabilizing the mode frequency [18] and repetition rate, respectively. We are now aiming at determining the spectral intervals of $6S$–$6D$ hyperfine transitions with better than 1 kHz accuracy.

We are grateful to Ming-Sheng Chang for kindly commenting on this paper, Jow-Tsong Shy for useful discussions, and Jon Hougen for the English corrections. This research is funded by the National Science Council of Taiwan (NSCT) under project NSC 94-2112-M-001-022-MY3.

References

1. For cesium atom: T. Ohtsuka, N. Nishimiya, T. Fukuda, and M. Suzuki, J. Phys. Soc. Jpn. **74**, 2487 (2005).
2. Professor Nobuo Nisimiya, Tokyo Polytechnic University, Atsugi-City, Kanagawa, 243-0297 Japan, nisimiya@em.t-kougei.ac.jp (personal communication, November 8, 2010).
3. M. Gunawardena, D. S. Elliott, M. S. Safronova, and U. Safronova, Phys. Rev. A **75**, 022507 (2007).
4. Y.-C. Lee, H.-C. Chui, Y.-Y. Chen, Y.-H. Chang, and C.-C. Tsai, Opt. Commun. **283**, 1788 (2010).
5. For rubidium atom, 778 nm standard: C. S. Edwards, G. P. Barwood, H. S. Margolis, P. Gill, and W. R. C. Rowley, Metrologia **42**, 464 (2005), and references therein.
6. For cesium: G. Hagel, C. Nesi, L. Jozefowski, F. Nez, and F. Biraben, Opt. Commun. **160**, 1 (1999).
7. For rubidium: M. Poulin, C. Latrasse, D. Touahri, and M. Tetu, Opt. Commun. **207**, 233 (2002). The cavity enhancing scheme is the most popular scheme to save power. It could be compact; however, optical feedback directly from the cavity is serious. More optical isolation and electronics are needed, which added to the cost and complexity.
8. C.-Y. Cheng, C.-M. Wu, G.-B. Liao, and W.-Y. Cheng, Opt. Lett. **32**, 536 (2007).
9. L. Ricci, M. Weidemuller, T. Esslinger, A. Hemmerich, C. Zimmermann, V. Vuletic, W. Konig, and T. W. Hansch, Opt. Commun. **117**, 541 (1995).
10. W. T. Hill, III, T. W. Hansch, and A. L. Schawlow, Appl. Opt. **24**, 3718 (1985).
11. W. Jamroz, D. Hugon, T. B. Cave, A. Guest, and A. D. May, Appl. Opt. **23**, 2906 (1984), and references therein.
12. Z. Bozoki, J. Sneider, G. Szabo, A. Miklos, M. Serenvi, G. Nagy, and M. Feher, Appl. Phys. B **63**, 399 (1996).
13. G. Stephan, R. Le Naour, and A. Le Floch, Phys. Rev. A **17**, 733 (1978).
14. P. Cerez and R. Felder, Appl. Opt. **22**, 1251 (1983).
15. S. T. Dawkins, J. J. McFerran, and A. N. Luiten, IEEE. Trans. Ultrason. Ferroelect. Freq. Contr. **54**, 918 (2007). We used an Agilent 53132A counter here, which is a lambda-type counter, and our beat note was around 160 MHz.
16. P. Fendel, D. Bergeson, Th. Udem, and T. W. Hansch, Opt. Lett. **32**, 701 (2007).
17. V. Gerginov, A. Deerevianko, and C. E. Tanner, Phys. Rev. Lett. **91**, 072501 (2003).
18. W.-Y. Cheng, T. H. Wu, S. W. Huang, S. Y. Lin, and C. M. Wu, Appl. Phys. B **92**, 13 (2008).